Biochimica et Biophysica Acta 1798 (2010) 167–176

Contents lists available at ScienceDirect

Biochimica et Biophysica Acta

journal homepage: www.elsevier.com/locate/bbamem

Suppressed or recovered intensities analysis in site-directed ^{13}C NMR: Assessment of low-frequency fluctuations in bacteriorhodopsin and D85N mutants revisited

Hazime Saitô [a,b,*], Atsushi Kira [a,c], Tadashi Arakawa [a], Michikazu Tanio [a], Satoru Tuzi [a], Akira Naito [c]

[a] Department of Life Science, Himeji Institute of Technology, University of Hyogo, Harima Science Garden City, Kamigori, Hyogo 678-1297, Japan
[b] Center for Quantum Life Sciences, Hiroshima University, Kagamiyama, Higashi-Hiroshima, 739-8526, Japan
[c] Faculty of Engineering, Yokohama National University, Hodogaya-ku, Yokohama 240-8501, Japan

ARTICLE INFO

Article history:
Received 6 February 2009
Received in revised form 8 June 2009
Accepted 30 June 2009
Available online 15 July 2009

Keywords:
Low-frequency dynamics
SRI analysis
Site-directed 13C NMR
Bacteriorhodopsin
D85N mutant site-directed 13C NMR

ABSTRACT

The first proton transfer of bacteriorhodopsin (bR) occurs from the protonated Schiff base to the anionic Asp 85 at the central part of the protein in the L to M states. Low-frequency dynamics accompanied by this process can be revealed by suppressed or recovered intensities (SRI) analysis of site-directed ^{13}C solid-state NMR spectra of 2D crystalline preparations. First of all, we examined a relationship of fluctuation frequencies available from [1-^{13}C]Val- and [3-^{13}C]Ala-labeled preparations, by taking the effective correlation time of internal methyl rotations into account. We analyzed the SRI data of [1-^{13}C]Val-labeled wild-type bR and D85N mutants, as a function of temperature and pH, respectively, based on so-far assigned peaks including newly assigned or revised ones. Global conformational change of the protein backbone, caused by neutralization of the anionic D85 by D85N, can be visualized by characteristic displacement of peaks due to the conformation-dependent ^{13}C chemical shifts. Concomitant dynamics changes if any, with fluctuation frequencies in the order of 10^4 Hz, were evaluated by the decreased peak intensities in the B–C and D–E loops of D85N mutant. The resulting fluctuation frequencies, owing to subsequent, accelerated dynamics changes in the M-like state by deprotonation of the Schiff base at alkaline pH, were successfully evaluated based on the SRI plots as a function of pH, which were varied depending upon the extent of interference of induced fluctuation frequency with frequency of magic angle spinning or escape from such interference. Distinguishing fluctuation frequencies between the higher and lower than 10^4 Hz is now possible, instead of a simple description of the data around 10^4 Hz available from one-point data analysis previously reported.

1. Introduction

Naturally, membrane proteins embedded in fluid biomembranes are susceptible to low-frequency motions at ambient temperature. Bacteriorhodopsin (bR) from the purple membrane (PM) of *Halobacterium salinarum* is a light-driven proton pump that translocates protons from the inside to the outside of the cell. It consists of seven transmembrane α-helices, A through G, enclosing an all-*trans* retinal covalently linked to Lys 216 in the helix G through a protonated Schiff base (Scheme I) [1–4]. The reaction cycle that follows photoisomerization of the retinal 13-*cis*, 15-*anti* is described by the sequence of intermediate states J, K, L, M, N, and O [1,2]. The first proton transfer occurs from the protonated Schiff base to the anionic Asp 85 at the central part of the protein in the L- to M-reaction [3] (Scheme II→III). Protonation of Asp 85 induces the release of a proton from the proton releasing group involving Glu 194 and Glu 204. Subsequently, the N state is formed by the reprotonation of the Schiff base from Asp 96, followed by the proton uptake to Asp 96 from the cytoplasmic surface [4–6]. Global conformational changes of the protein backbone occur in the M and/or N intermediates together with the deprotonated and reprotonated Schiff base, respectively, as observed by neutron [7,8], X-ray [9–14], and electron diffraction studies [15–17]. Such global conformational changes may be part of the proton access switch between the deprotonation and reprotonation of the Schiff base [18,19].

Bacteriorhodopsin in the membrane is known to form hexagonal arrays [20], leading to a 2D crystalline lattice through its oligomerization to the trimeric form [21]. Nevertheless, we demonstrated that bR structure is far from being a rigid body at *ambient temperature* even in the 2D crystalline state, as viewed from site-directed NMR [22–28], in spite of its static 3D structural models determined by cryo-electron microscope or X-ray diffraction studies at *lower temperature* [13,14, 29–33]. Indeed, the dynamic feature of this protein turned out to be highly heterogeneous, with correlation times in the order of 10^{-2}–10^{-8}s as viewed from comparative ^{13}C magic angle spinning (MAS) NMR with and without cross polarization (CP) and suppressed peaks due to interference of MAS and fluctuation frequencies, depending upon various portions from transmembrane helices, through loops, to N- or C-terminal residues [22,23,27,28]. In particular, the presence of isotropic or large-amplitude motions, with fluctuation

* Corresponding author. Department of Life Science, Himeji Institute of Technology, Harima Science Garden City, Kamigori, Hyogo, 6781297, Japan.
E-mail address: hsaito@siren.ocn.ne.jp (H. Saitô).

0005-2736/$ – see front matter © 2009 Elsevier B.V. All rights reserved.
doi:10.1016/j.bbamem.2009.06.027

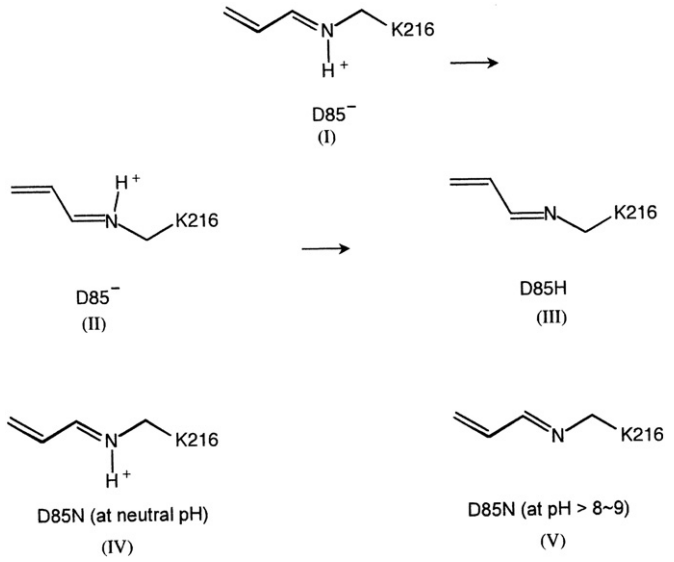

Scheme 1.

frequency in the order 10^8 Hz as in the N- or C-terminal residues, can be readily identified by their selectively suppressed peaks in CP-MAS NMR spectra, as compared with peaks observed by single-pulse dipolar decoupled-MAS (DD-MAS) NMR spectra [22,27,28]. On the contrary, the presence of the slow motions of 10^4 to 10^5 Hz (or 10^{-4} to 10^{-5} s as correlation times) in membrane proteins can be readily confirmed by examination of the suppressed peaks both in the ^{13}C CP-MAS and DD-MAS NMR [34–39], which are caused by interference of motional frequencies with frequencies of proton-decoupling or magic angle spinning [40,41]. Such slow motions of the backbone and side-chains on a time scale of millisecond and microsecond, have been pointed out to be biologically relevant for the specific activity of a variety of globular proteins in solution. This includes transient formation of ligand-binding-competent states and transitions coupled to enzyme catalysis where fast motions are detectable by relaxation parameters [42–44]. This is particularly true for a variety of membrane proteins embedded in biomembranes [22,23,27,28].

Particular conformations of membrane proteins at the site of interest can be readily assessed by comparison of their ^{13}C chemical shifts with the conformation-dependent ^{13}C chemical shifts [27,28,45–47]. This approach is only possible when the ^{13}C NMR signals have been assigned in advance, and are fully visible as in the spectra of 2D crystalline preparations. For this purpose, unequivocal assignment of peak to a certain specific residue is possible by looking at the reduced peak intensity, owing to lacking such signal from site-directed mutant where the residue under consideration is replaced by another, with reference to ^{13}C NMR spectra of [3-^{13}C]Ala- and [1-^{13}C]Val-labeled bR of wild type [27,28,34,35]. Nevertheless, it should be taken into account that such necessary information is not always available from the preparations of monomeric bR [36,37] because the presence of such suppressed peaks, if any, tends to be masked by the accompanied spectral change owing to the onset of the low-frequency fluctuations in the absence of crystalline lattice. For this reason, bR in the 2D crystalline state can be considered as a very useful model system for a variety of membrane proteins, especially as a prototype of G-protein coupled receptors (GPCRs).

In our continuing effort to reveal bR dynamics in relation to its functions, we previously recorded ^{13}C NMR spectra of [1-^{13}C]Val-labeled D85N, D85N/D96N, and D85N/V49A mutants (Scheme IV and V instead of II and III), to reveal possible low-frequency fluctuation

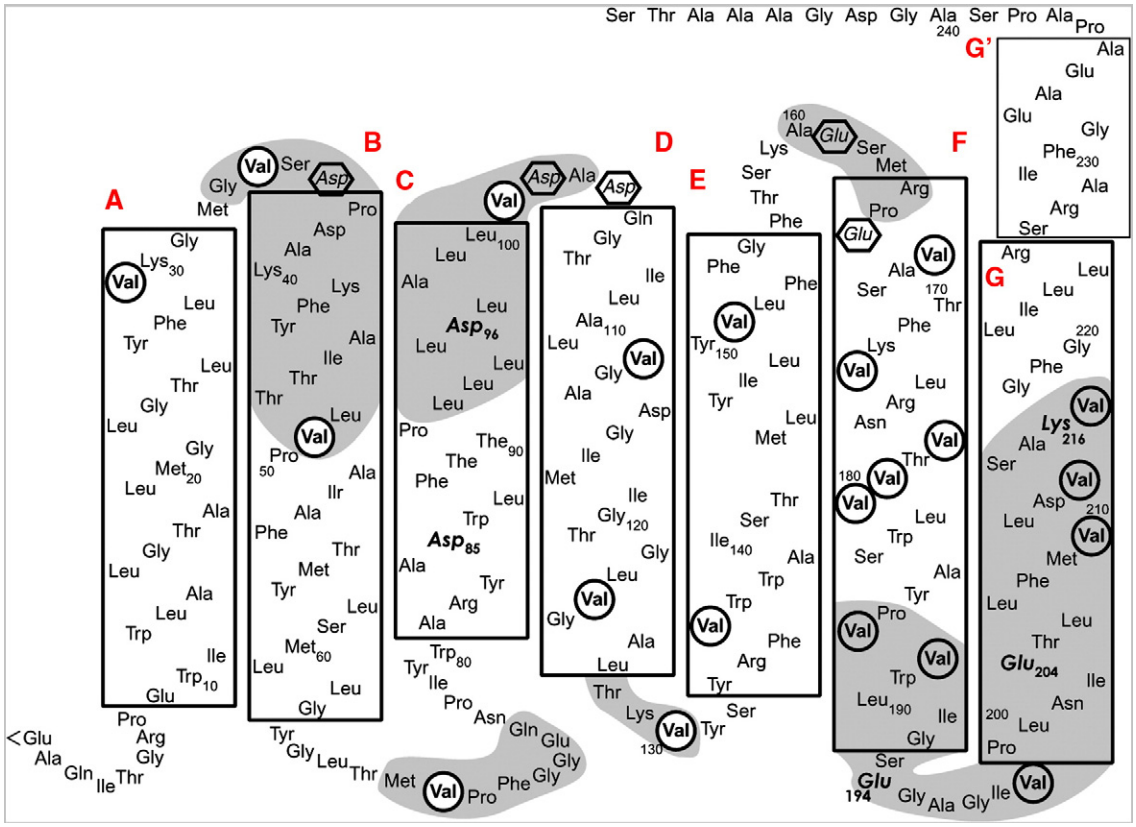

Fig. 1. Schematic representation of amino-acid residues involved in bacteriorhodopsin by taking into account the secondary structure based on X-ray diffraction [13]. Individual transmembrane α-helices are marked by the symbols A–G and the cytoplasmic α-helix protruding from the bilayer is marked by G'. Asp and Glu residues in the hexagons at the cytoplasmic site are located at the proton conducting channel, while Glu 194 and Glu 204 at the extracellular site are involved in the proton releasing complex. Chromophore is linked to Lys 216 by formation of Schiff base. Regions undergoing low-frequency fluctuation motions in the M-like state were shaded.

motions [48,49]. This is because these mutants are very useful for studying the M-like state without photo-illumination (Scheme V) because the pK_a of the Schiff base is lowered from >13 to 8–9 by the replacement of Asp 85 with a nonionic residue, which is essential for the M-like state [18]. In the present paper, we attempted to re-examine the abovementioned spectral data by careful examination of the SRI plots against pH, based on so-far assigned peaks including newly assigned [35] or revised peaks [50]. It turned out that more detailed fluctuation frequencies can be obtained from these kinds of plots rather than one point analysis previously reported.

2. Materials and methods

[1-^{13}C]valine was purchased from Cambridge Isotope Laboratories (Andover, USA) and used without further purification. BR mutants, D85N, D85N/D96N, and D85N/V49A (see Fig. 1, as to their positions) were provided by Professors J. K. Lanyi of University of California, Irvine, CA, USA and R. Needleman of Wayne State University, MI, USA. *H. Salinarum* S9 (wild-type bR) and these mutants were grown in temporary synthetic (TS) medium of Onishi et al. [51], in which unlabeled L-valine was replaced by L-[1-^{13}C]valine. Purple membranes from these sources were isolated by the method of Oesterhelt and Stoeckenius [52] and suspended in 5 mM HEPES buffer (pH 7) containing 0.025% (w/v)NaN_3 and 10 mM NaCl at pH 7. PMs were spun down at 40,000×*g* for 1 h. Samples for ^{13}C NMR measurements were placed into a 5 mm outer diameter zirconia pencil-type rotor for magic angle spinning (MAS). To prepare deionized blue membrane, PM resuspended in distilled water was treated with cation exchange resin Dowex 50W-X8 until the absorption maximum of the chromophore shifted from 568 to 603 nm [53]. The pH value of the deionized blue membrane was 4. Regenerated PM was prepared by adding 10 mM NaCl to the deionized blue membrane resuspended in 5 mM HEPES buffer. Sample rotors were tightly sealed by Teflon caps and the caps were glued to the rotor by rapid epoxy resin to prevent dehydration of pelleted samples through any pin-hole in the caps during MAS experiment under a stream of dried compressed air.

^{13}C NMR spectra were recorded at 100.64 MHz usually at ambient temperature (20 °C) and also at lower (0 °C) and higher (40 °C) temperatures in the dark using standard CP-MAS method. The spectral width, contact, repetition, and acquisition times were 40 kHz, 1 ms, 4 s, and 50 ms, respectively. Free induction decays (FIDs) were acquired by 2 k data points and Fourier-transformed as 16 k data points after 14 k data points were zero-filled, after accumulation of FIDs more than 5000 times. The $\pi/2$ pulses for carbon and proton were 5.0 μs and the spinning rate was 4 kHz. ^{13}C chemical shifts were referred to the carboxyl signals of glycine (176.03 ppm) and then converted to values with reference to tetramethylsilane (TMS).

3. The SRI factor as a means to detect low-frequency motions

Local or global dynamics can be easily characterized by either change of a single or several peak intensities [45,46]. Indeed, a ^{13}C NMR line width $1/\pi T_2^C$ of the residue under consideration could be considerably broadened, when a motional frequency of incoherent random fluctuation motion is interfered with either coherent frequency of the proton-decoupling or magic angle spinning [40,41]. In such cases, the overall transverse relaxation rate $1/T_2^C$ can be dominantly determined by the following second or third terms, instead of the first term of static component, in the case of resting state, by [54]

$$1/T_2^C = (1/T_2^C)^S + (1/T_2^C)_{DD}^M + (1/T_2^C)_{CS}^M, \quad (1)$$

where $(1/T_2^C)^S$ is the transverse component due to static C–H dipolar interactions, and $(1/T_2^C)_{DD}^M$ and $(1/T_2^C)_{CS}^M$ are the transverse components due to the fluctuation of dipolar and chemical shift interactions

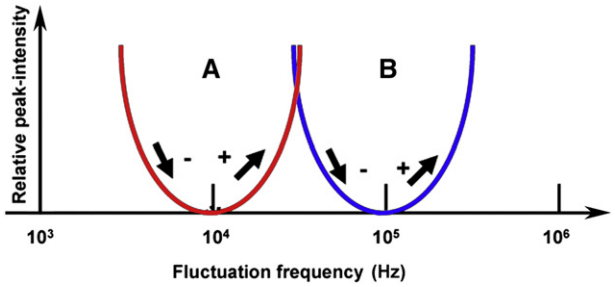

Fig. 2. Plots of SRI data, owing to interference of motional frequency with frequency of MAS (10^4 Hz, A) or proton-decoupling (10^5 Hz, B), against the fluctuation frequency. The symbols, − and +, stand for the decreased or increased peaks, respectively.

in the presence of internal fluctuation motions, respectively. The latter two terms are given as a function of the correlation time τ_c by

$$(1/T_2^C)_{DD}^M = \Sigma(4\gamma_I^2\gamma_S^2\hbar^2/15r^6)I(I+1)\left[(\tau_c/(1+\omega_I^2\tau_c^2))\right], \quad (2)$$

$$(1/T_2^C)_{CS}^M = (\omega_0^2\delta^2\eta^2/45)\left[\tau_c/(1+4\omega_r^2\tau_c^2) + 2\tau_c/(1+\omega_r^2\tau_c^2)\right]. \quad (3)$$

Here, γ_I and γ_S are the gyromagnetic ratios of I (proton) and S (carbon) nuclei, respectively, and r is the internuclear distance between spins I and S. ω_0 and ω_I are the carbon resonance frequency and the amplitude of the proton-decoupling RF field, respectively. ω_r is the rate of spinner rotation. δ is the chemical shift anisotropy and η is the asymmetric parameter of the chemical shift tensor. It is expected that a decoupling field of 50 kHz is sufficient to reduce the static component and the $(1/T_2^C)_{CS}^M$ term will be dominant in the overall $1/T_2^C$, as far as the carbonyl signals with larger chemical shift anisotropies are concerned. Consequently, the maximum of the line-broadening appeared at the incoherent motional frequency near ω_r, which is called interference of motional frequency with the MAS frequency. Of course, it is possible to avoid the abovementioned interference with frequency in the order of 10^4 Hz by increasing the spinning rate up to as fast as 20 kHz. In such case, however, one should take special precaution to prevent unnecessary heating of samples as well as dehydration due to centrifuging effect on fully hydrated membrane proteins.

A very rough sketch of how ^{13}C NMR peak intensities vary with fluctuation frequency based on the Eqs. (2) and (3) is drawn in Fig. 2, as the SRI plots exhibiting the presence of such low-frequency motions. Namely, a peak intensity of [1-^{13}C]Val-labeled bR or its mutants of the 2D crystalline lattice, for instance, could be suppressed (↘ or -) when motional frequency was increased from 10^3 to 10^4 Hz (Fig. 2A) because such suppressed peaks are available from interference with the MAS frequency in the vicinity of 10^4 Hz. Furthermore, the peak intensity which is once suppressed will be recovered (↗ or +) when the motional frequency is increased from 10^4 to 10^5 Hz. In practice, the SRI plots are experimentally available from the observed ^{13}C NMR peak intensities as a function of either temperature or pH, which can be related to possible fluctuation frequencies for the site of interest, to be shown below.

The SRI minimum as viewed from the ^{13}C NMR signal of [3-^{13}C]Ala-bR, however, occurs at the motional frequency around 10^5 Hz due to the interference with the proton-decoupling frequency (40 kHz) as shown in the trace in Fig. 2(B). Note that this occurs when the correlation time on internal rotation of methyl group τ_i leads to modify its correlation time τ_m. The effective local correlation time τ_C is thus given by Eq. (4), if this motion is described by random jumps between three equilibrium positions at an average rate of $(3\tau_i)^{-1}$ [55–57],

$$\tau_c = (1/4)(3\cos^2\theta - 1)2\tau_m + (3/4)(\sin^2 2\theta + \sin^4\theta)(1/\tau_m + 1/\tau_i)^{-1}, \quad (4)$$

where θ is the angle between the rotation axis and C–H bond axis. Because θ is equal to the tetrahedral angle,

$$\tau_c = 0.11\tau_m + 0.89(1/\tau_m + 1/\tau_i)^{-1}. \quad (5)$$

If $\tau_i \ll \tau_m$ as in the case of alanine residues in the solid [58], Eq. (5) can be simplified to

$$\tau_c = 0.11\,\tau_m. \quad (6)$$

Therefore, the backbone fluctuation frequency ($1/\tau_C$) in the order of 10^4 Hz as viewed from [1-^{13}C]Val-labeled protein could be detected by the fluctuation frequency in the order of 10^5 Hz when [3-^{13}C]Ala-labeled protein was utilized as a probe as demonstrated in Fig. 2B.

It is noted that these critical frequencies could be varied with use of either higher MAS frequency or higher power of proton-decoupling. Therefore, further experiments under such conditions are undoubtedly very important. Furthermore, it is pointed out that this kind of obvious spectral changes cannot be expected when monomeric preparations unable to form 2D crystalline lattice were utilized because such low-frequency motion, if any, could be masked by overall motions in membrane proteins [36,37]. In any case, this SRI factor can be a very sensitive tool to be able to detect a portion whose flexibility is changed without changing local structures. It is noted that slow motions of similar time scale can be also detected by dipolar and chemical shift correlation experiments [59,60].

4. Results

Our site-directed NMR approach starts from the assignment of peaks, and subsequent conformational characterization can be made based on the conformation-dependent ^{13}C chemical shifts [45,46]. The presence of low-frequency protein dynamics can be further revealed by locating the peaks exhibiting SRI due to either interference of such frequency with MAS or proton-decoupling frequencies [40,41] or escape from such interference.

4.1. Temperature-dependent ^{13}C NMR spectra of wild-type [1-^{13}C]Val-bR

In relation to the interpretation of such reduced peak intensity, we examined whether such low-frequency motion could be detected for [1-^{13}C]Val-labeled wild-type bR, by recording its ^{13}C CP-MAS NMR spectra at various temperatures, from 0 °C (A) through 20 °C (B) to 40 °C (C), as illustrated in Fig. 3. Interestingly, the peak intensity at 172.93 ppm (V34) alone is substantially increased by raising temperature from 0 to 40 °C, while the peak intensity of the ^{13}C NMR signal at 174.01 ppm (V151, V167 and V180) was simultaneously decreased to some extent. On the contrary, the peak intensity at 171.07 ppm (V101 and V199) remains unchanged with the temperatures. These spectral changes can be unequivocally interpreted in terms of the recovery of the rather flexible V34 (the A–B loop) at ambient temperature, even if this peak was suppressed at low temperature. This temperature dependence indicates that the motional frequency of V34 (the A–B loop) alone is higher than 10^4 Hz at ambient temperature, while those of V151, V167, and V180 (helix) are lower than 10^4 Hz. In other word, the fluctuation frequency of the A–B loop alone as viewed from the V34 signal is located at the right-hand side of the intensity minimum ($>10^4$ Hz), although the rest loops take the fluctuation frequency at the left-hand side ($<10^4$ Hz) (Fig. 2A). In fact, the fluctuation frequency of V167 at the corner of the transmembrane α-helix appears at the left-hand side of the minimum

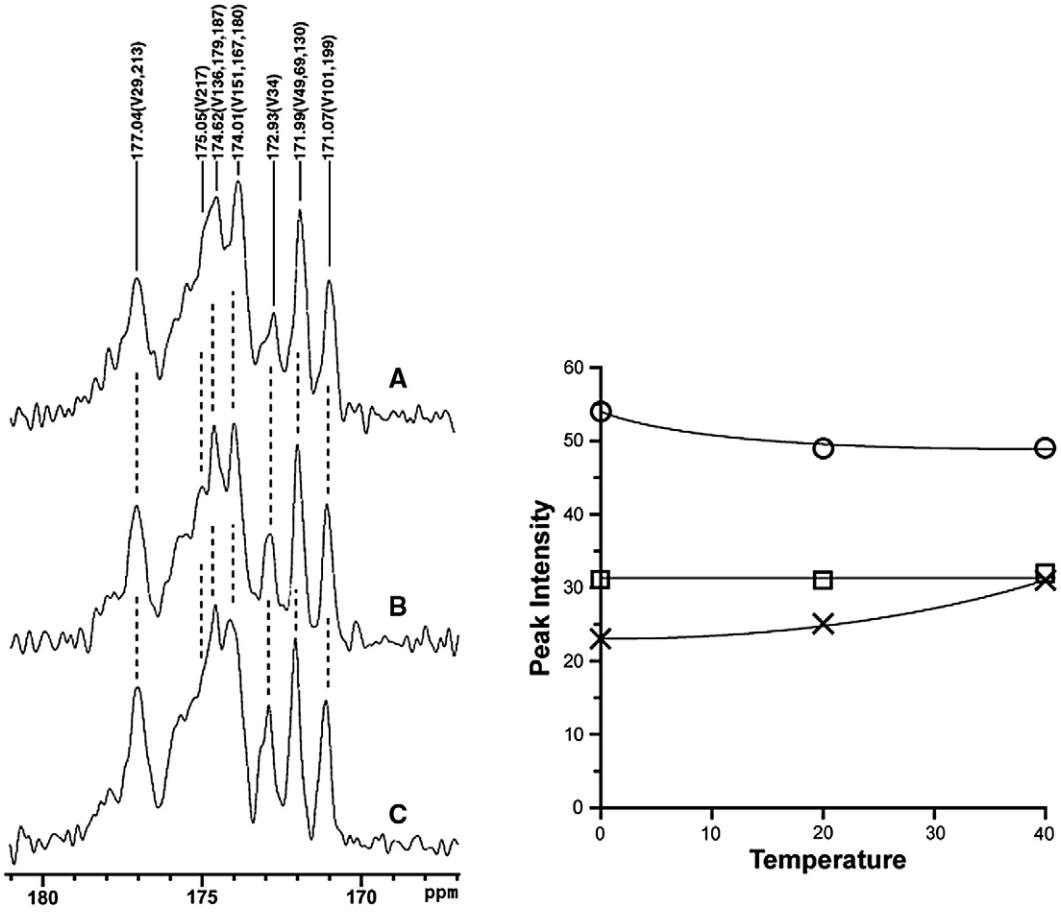

Fig. 3. The 100.6 MHz ^{13}C CP-MAS NMR spectra of [1-^{13}C]Val-labeled wild-type bR at various temperatures. (A) 0 , (B) 20 , and (C) 40 °C (left). SRI plots of some bR peaks against temperature (right). ○,174.01 ppm (V151, 167, 180); □,171.07 ppm (V101, 199); ×,172.93 ppm (V34).

but the rest of the helices are in the order of 10^2 Hz [61]. The slightly decreased peak together with the temperature should be ascribed to V167 which is located at the corner of the helix F, and more susceptible for temperature-dependent fluctuation motions as compared with V151 and V180 located at the transmembrane α-helices. It is mentioned here that such temperature-dependent spectral changes are more pronounced for ^{13}C DD-MAS NMR spectra of flexible side-chain carbons of swollen poly(acrylate)s (Y. Miwa, H. Ishida, H. Saitô, M. Tanaka, and A. Mochizuki, submitted for publication).

4.2. Spectral changes of bR by neutralization of aspartic acid 85 near at the Schiff base

In Fig. 4, we illustrate the ^{13}C NMR spectra of [1-^{13}C]Val-labeled bR (A), D85N mutant (B), deionized blue membrane (C), and regenerated PM from the blue membrane (D), together with their assignment of peaks so-far achieved [35] and recently corrected by REDOR filtered experiments [50]. It is noted that the global conformational and dynamic changes in D85N mutant (Fig. 4B) are triggered by the neutralization of D85 as D85N alone as compared with bR (Fig. 4A): the four asterisked ^{13}C NMR signals of D85N (at 172.30 [V49 (helix B)], 173.19 [V34 (A–B loop)], 175.05 [V217 (helix G) and one of V136 (helix E), V179 (helix F), or V187 (helix F)], and 177.67 ppm [displaced V29 (helix A) or V213 (helix G)]) were displaced downfield, together with the reduced peak intensities at 172.03 ppm (V69/130; B–C/D–E loop) and 177.04 ppm (V29 or V213). Obviously, the B–C and D–E loops

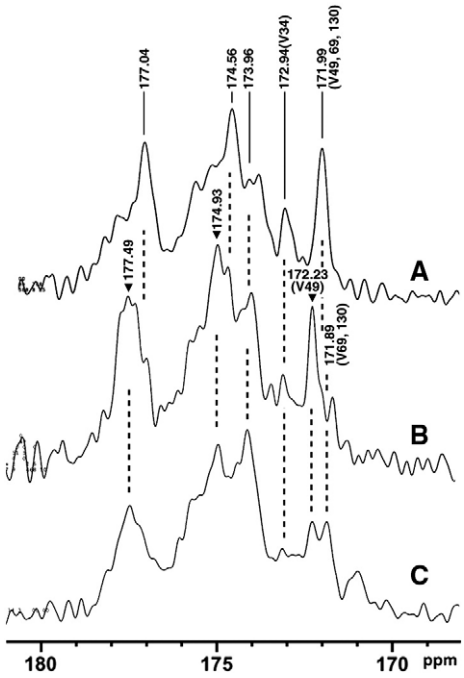

Fig. 5. The 100.6 MHz ^{13}C CP-MAS NMR spectra of [1-^{13}C]Val-labeled bR (A), D85N mutant at pH 7 (B), and at pH 10 (C) all in the presence of 40 μM Mn^{2+} ion.

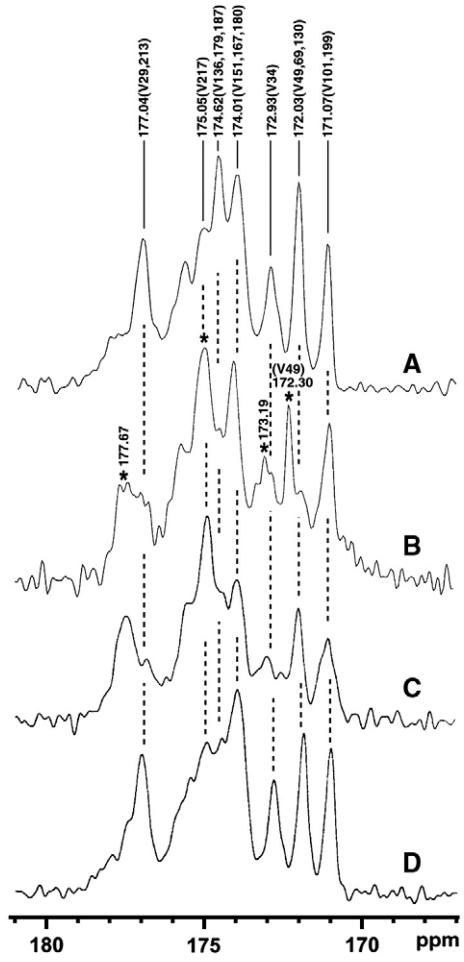

Fig. 4. The 100.6 MHz ^{13}C CP-MAS NMR spectra of [1-^{13}C]Val-labeled wild-type bR (A), D85N mutant at pH 7(B), deionized blue membrane (C), and regenerated PM from the blue membrane by addition of 10 mM NaCl (D). The assigned peaks so far achieved were also indicated [38,50]. The asterisked peaks in D85N are shown by the displaced peaks as compared from bR.

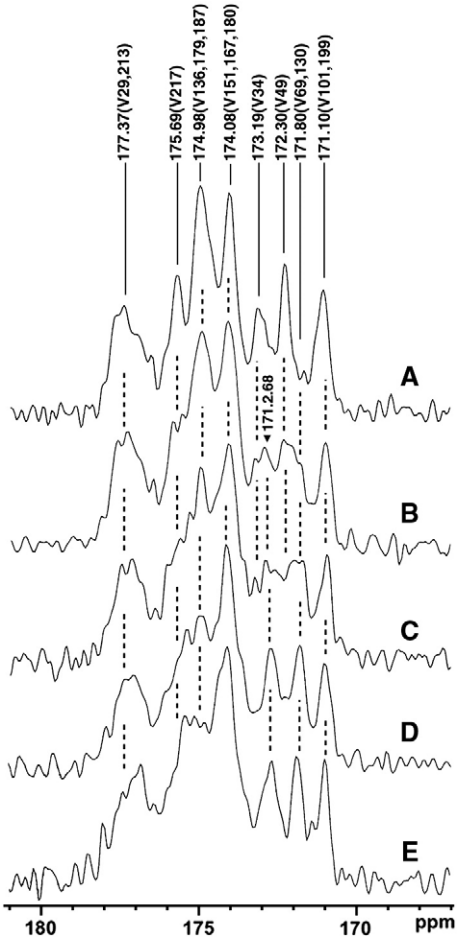

Fig. 6. The 100.6 MHz ^{13}C CP-MAS NMR spectra of [1-^{13}C]Val-labeled D85N mutant at various pH values: pH 6 (A), 8 (B), 9 (C), 10 (D), and 11 (E). The assignment of peaks is based on newly performed [35] and corrected ones [50].

undergo fluctuation motions with a frequency of 10^4 Hz as viewed from the suppressed V69/130 peak intensity, as far as ^{13}C NMR data on [1-^{13}C]Val-labeled preparations were concerned. Here, the accidentally overlapped ^{13}C signal from the three residues V49/69/130 at 172.03 ppm from wild-type bR is split into the two peaks at 172.23 and 171.89 ppm for D85N after the addition of 40 μM Mn^{2+} ion, as shown in Fig. 5 (C). As already pointed out, the ^{13}C NMR signals of the residues located within 8.7 Å from the surface are suppressed by fast relaxation effect by Mn^{2+} ion [62]. Therefore, the displaced peak at 172.30 ppm of D85N is assigned to V49 because this residue is located at the inner portion of the transmembrne α-helices and its signal is not affected by Mn^{2+} ion.

Furthermore, it is interesting to note that the observed spectral pattern of D85N is very similar to that of the deionized blue membrane, except for the peak position and intensity of V49/V69/V130 (Fig. 4C). This spectral pattern is nearly recovered to that of native purple membrane (PM), when the regenerated PM from the blue membrane was prepared by addition of 10 mM NaCl (without divalent cations) as shown in Fig. 4D. The purple to blue transition, with altered photocycle and no proton pump activity [63,64], is caused by lowering surface pH to 4 [65,66] to remove cations present in the protein or membrane surfaces. Therefore, it is surprising to note that the ^{13}C NMR spectral pattern of [1-^{13}C]Val-D85N (Fig. 4B) is very similar to that of the deionized blue membrane (Fig. 4C), except for the peak positions of V49/V69/V130 and also the intensity at 174.62 ppm. For the sake of assignment of displaced ^{13}C NMR peaks

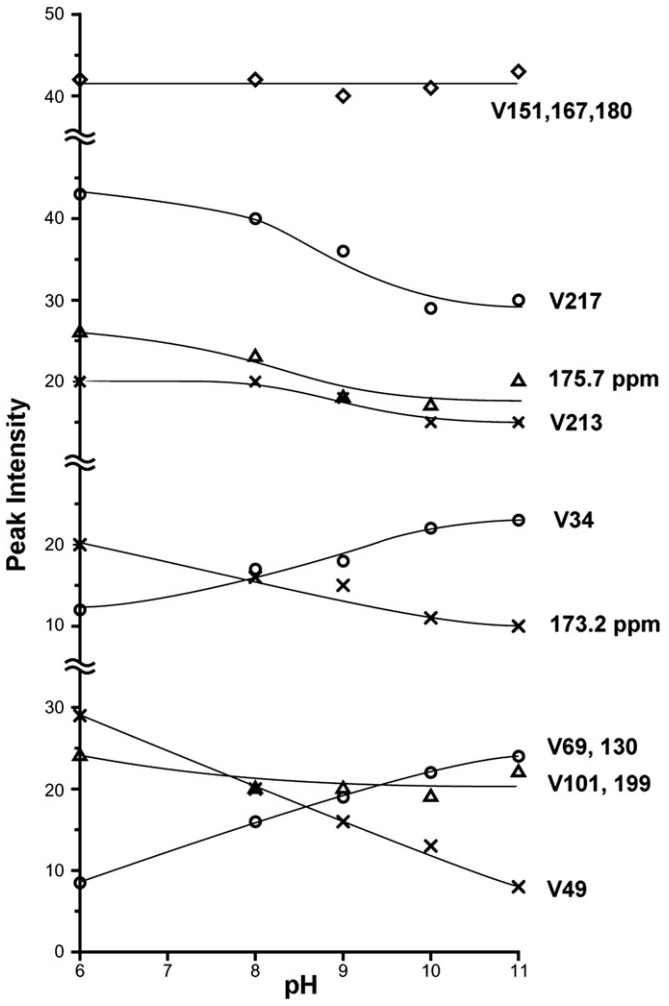

Fig. 7. SRI plots for D85N mutant against pH. The peak intensities are either increased or decreased together with the increased pH, depending upon the respective peaks, except for the peak V151, 167, 180 whose intensity was unchanged.

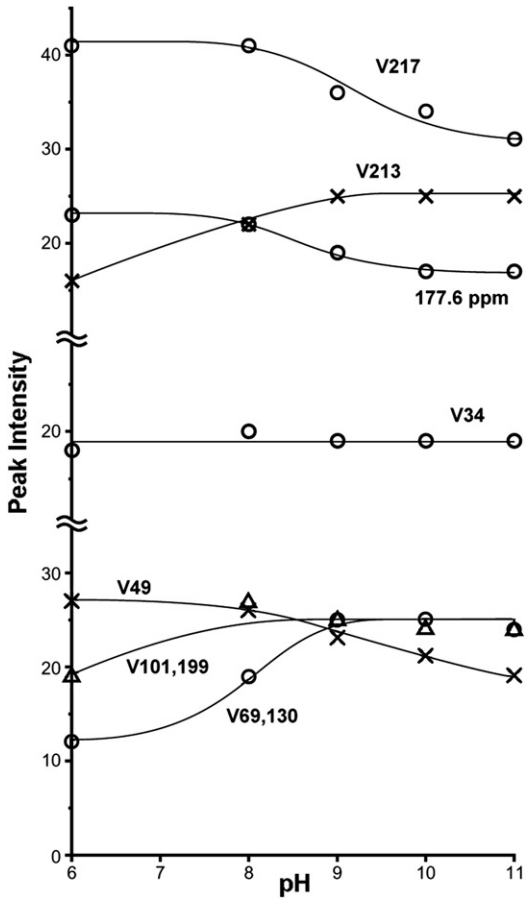

Fig. 8. SRI plots for D85N/D96N mutant against pH. In contrast to the data on D85N, the peak intensity for V34 of this mutant is unchanged, regardless of the pH values.

for D85N mutant, we compared the ^{13}C NMR peaks of D85N at pH 7 (Fig. 5B) and 10 (Fig. 5C) with those of wild-type bR (Fig. 5A) all in the presence of 40 μM Mn^{2+} ion. It is noteworthy that the displaced peak at 172.23 ppm can be undoubtedly ascribed to V49, although most of the signals from the loops were suppressed by the added Mn^{2+} ion (see Fig. 5B). In addition, the peak intensity of V49 was decreased in the M-like state achieved at pH 10, whereas the once suppressed peak at 171.89 ppm ascribable to V69 and 130 was partially recovered at pH 10 by escape from once suppressed peak at neutral pH.

4.3. pH-dependent spectral changes: [1-^{13}C]Val-D85N, D85N/D96N, and D85N/V49A

To further examine this point, we demonstrate the previously published ^{13}C NMR spectra of [1-^{13}C]Val-labeled D85N recorded at pH 6, 8, 9, 10, and 11, together with the assigned so-far [27,28,35] and recently corrected peaks [50], as shown in Fig. 6. Raising pH from 7 to 10 (M-like state) resulted in additional spectral changes in which several peaks were suppressed together with raising pH to 10, while the others were recovered. For the sake of comparison, the intensities of the individual peaks for D85N were plotted against pH as shown in Fig. 7. To justify such a plot, it is noted that there exist a few peaks [171.10 ppm (V101 and V199) and 174.08 ppm (V151, 167, 180)] whose intensities were almost unchanged irrespective of pH, and they can be used as reference peaks for the intensity comparison. Obviously, the removal of the electrostatic Schiff base-counter ion interaction due to deprotonation of the Schiff base (V) leads to global low-frequency fluctuation motions in the M-like state. In particular, the intensities of the five peaks in D85N, 177.31 ppm (V213), 175.69 ppm (unassigned), 174.98 ppm (V217), 173.2 ppm (unassigned), and 172.3 ppm (V49),

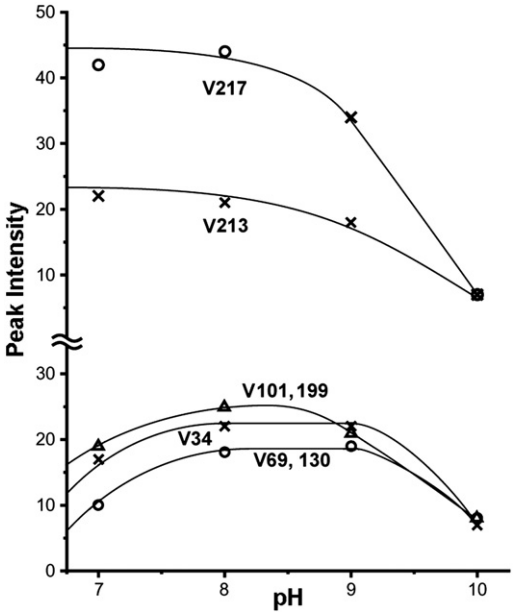

Fig. 9. SRI plots for D85N/V49A mutant against pH. It is noteworthy that the decreased (V217 and V213) or increased (V34, V69, 130 and V101, 199) peaks together with the increased pH are finally suppressed at pH 10.

were decreased with the raised pH, while the intensities of the two peaks, 171.8 ppm (V69,130) and 172.8 ppm (V34), were increased. Of course, such SRI data can be related with the suppressed [the left-hand side (-)] and recovered [right-hand side (+)] peaks, as schematically represented in Fig. 2A, by taking into account that raising pH is related to the increased fluctuation frequency as a result of conformational change from the L- to M-like state of bR.

A similar plot for D85N/D96N mutant (from [47], Fig. 6) in Fig. 8 shows that the intensities of the three kinds of peaks from D85N/D96N mutant, 177.55 ppm (V213), 174.82 ppm (V217), and 172.36 ppm (V49), were decreased with the raised pH, while the peak intensities of the three peaks, 177.0 ppm (V213), 171.86 ppm (V69, V130), and 170.94 ppm (V101 and V 199), were increased. It is noted that the peak intensity at 172.82 ppm (V34) remained unchanged for D85N/D96N mutant [49], however. Furthermore, Fig. 9 illustrates that the peak intensities of the two peaks from D85N/V49A mutant, 177.28 ppm (V213) and 174.85 ppm (V217), were decreased with the raised pH up to 8 and their intensities were further decreased at pH 10. On the contrary, the intensities of the three peaks from the cytoplasmic and extracellular loops of D85N/V49A [49], 171.02 ppm (V101 and V199) and 171.96 ppm (V69,130), and 172.87 ppm (V34), were increased together with pH up to 8–9 and then suppressed at pH 10.

Here, we summarized the SRI data of [1-^{13}C]Val-D85N mutants from the experimental plots (Figs. 7–9), together with the previous data from [3-^{13}C]Ala- [48,49] or [1-^{13}C]Pro-labeled mutants [61], as summarized in Table 1. Indeed, the fluctuation frequencies from the SRI data of similar sites obtained from both [1-^{13}C]Val- and [3-^{13}C]Ala-labeled D85N are consistent with each other, if the argument on the methyl rotation were taken into account as described by Eqs. (5) and (6). Therefore, it is emphasized that evaluating fluctuation frequency from both [1-^{13}C]Val- and [3-^{13}C]Ala-labeled preparations turned out to be a very convenient and useful complementary means to locate the portion of low-frequency dynamics.

5. Discussions

5.1. Global conformational changes of bR by replacement with D85N mutant: the effect of the neutralization of a counter ion to the Schiff base

It is notable from Figs. 4 and 6 that the global conformational change is immediately triggered by the removal of the electrostatic Schiff base–counter ion (anionic D85) interaction by replacement with D85N, as viewed from the displaced ^{13}C chemical shifts of D85N mutant as compared with those of bR (see Fig. 4). Indeed, the displacements of the peaks, V49 (helix B) and V69 (B–C loop), V34 (A–B loop), one of V136 (helix D), V 179(helix F), or V183 (helix F) and V29 (helix A) or V213 (helix G), are evident. Low-frequency fluctuation with 10^4 Hz frequency is also seen at V69/130 (A–B/D–E loops). These changes arose from a modified helix–helix interaction triggered by loss of electrostatic Schiff base-counter interaction. Therefore, it is tempted to gain insight into a possibility to relate such ^{13}C chemical shifts with the individual torsion angles available from 3D crystalline preparation [65], in order to gain insight into their structural features.

We thus plotted the ^{13}C NMR peaks of [1-^{13}C]Val -bR against the respective torsion angles (ϕ, φ) currently available from the X-ray diffraction study of 3D crystalline bR [67], as shown in Fig. 10. Experimentally, the ^{13}C peak positions of the transmembrane α-helices (black) and loop region (blue) are well-separated, except for the peak from Val49 residue whose chemical shift is strongly influenced by the neighboring Pro50 effect [66]. The following points should be borne in mind: first, the observed ^{13}C NMR peaks from the loop region, recorded at ambient temperature, cannot be strictly related to the torsion angles available from the low temperature study for X-ray diffraction. Indeed, the V101 ^{13}C signal exhibits the peak position of the loop regions, in spite of its torsion angles which are close to those of the α-helix at the low temperature for X-ray diffraction. In addition, the torsion angles themselves are not always accurate because of their larger thermal factors in X-rat diffraction data. This is because the observed ^{13}C NMR peaks are subject to a

Table 1
SRI data for the M-like state of D85N mutants[a].

	Transmembrane α-helices						Loops					
	B[b]	C	D	E	F	G	A–B	B–C[b]	C–D[c]	D–E	E–F	F–G[c]
D85N	A39(−) V49(−) A51(−) A53(−)	P91(−)	A126(−)		P186(−)	V213(−) A215(−) V217(−)	V34(+)	V69(+)	V101(0)	V130(+)	A160(−)	A196(−) V199(0)
D85N/D96N[d]	A39(−) V49(−) A51(−) A53(−)	P91(−)	A126(+)		P186(−)	V213(+) A215(−) V217(−)	V34(0)	V69(+)	V101(+)	V130(+)	A160(+)	A196(+) V199(+)
D85N/V49A[d]						V213(−) V217(−)	V34(+)		V101(+)	V130(+)		V199(+)

[a] The symbols, (−) and (+), stand for the suppressed and recovered peaks, respectively. The symbol (0) means unchanged. Data based on [48] (A residues), [61] (P residues), and [49] and this work (V residues).
[b] The peak positions for V49 and V69 are accidentally superimposed.
[c] The peak positions for V101 and V199 are accidentally superimposed.
[d] ^{13}C NMR measurements on [1-^{13}C]Pro-labeled preparations were not performed.

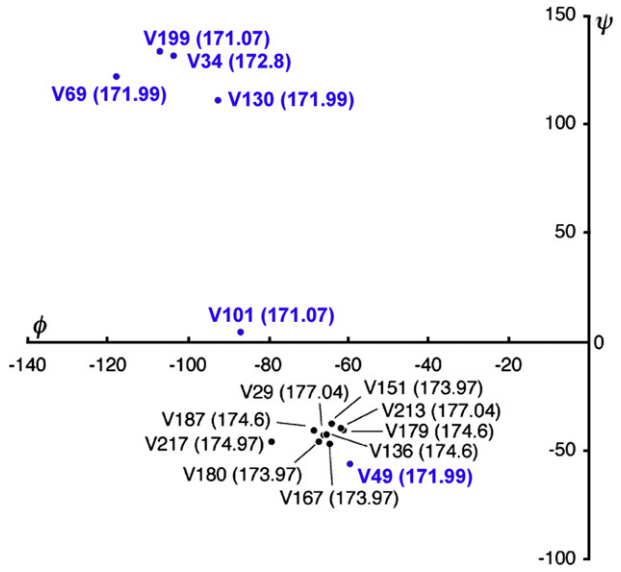

Fig. 10. A plot of the observed ^{13}C chemical shifts of individual residues in [1-^{13}C]Val-labeled bacteriorhodopsin against the respective backbone torsion angles available from X-ray diffraction data [67]. Residues exhibiting the ^{13}C chemical shifts corresponding to the α-helices are indicated by the black, while those corresponding to the loops are marked by the blue.

time-averaged structure consisting of several superimposed conformers undergoing fast chemical exchange. Therefore, the data points for the loop regions can be widely scattered in such plots. Furthermore, it appears that the carbonyl ^{13}C chemical shifts of the transmembrane α-helices arise also from the contribution of hydrogen bonding interactions with nearby residues, in addition to the contribution of the torsion angles, as pointed out already [68,69].

5.2. Global dynamics change in D85N, D85N/D96N, and D85N/V49A in the M-like state

Here, we briefly discuss the dynamic feature of wild-type bR, before proceeding to that of these mutants. As described above, the peak intensity of wild-type bR at 172.93 ppm (V34) was substantially reduced by lowering temperature from 40 to 0 °C, while the peak intensity at 173.97 ppm (V167) was simultaneously increased. The other peaks were unchanged irrespective of temperatures studied. This means that the low-frequency motions ($>10^4$ Hz) are present in the A–B loop region at 0 °C, whereas the low-frequency motions ($<10^4$ Hz) start in the E and F helices at 40 °C.

In the M-like state, we demonstrated that all the interhelical loops of [1-^{13}C]Val- and [3-^{13}C]Ala-labeled D85N mutant, except for the C–D loop, undergo the low-frequency fluctuation motions, as summarized in Table 1. In particular, the backbone carbons in the A–B, B–C, and D–E loops turned out to be involved in the low-frequency motions in the order of $>10^4$ Hz, while those of the E–F and F–G loops and transmembrane helices are in the order of $<10^4$ Hz. As pointed out already, identical results are available from the data of [1-^{13}C]Val- and [3-^{13}C]Ala-labeled preparations, if the relationship of the two correlation times, τ_m and τ_c, as discussed in Eq. (4) were taken into account. Furthermore, such motions for D85N/D96N mutant might be more accelerated in view of the recovered peaks, A126 (helix D), A196, and V199 (F–G loop), and the indicated change from the suppressed (−) to recovered (+) peaks (A160; E–F loop), as well as the abovementioned changes in D85N mutant. This means that the fluctuation motions present in D85N/D96N mutant are more accelerated than in D85N (see Table 1), in contrast to our previous interpretation [48,49]. The revised explanation is that the A126 and A160 peaks in D85N/D96N should be interpreted in terms of the recovered peak intensities in the presence of low-frequency motions ($>10^5$ Hz as viewed from the backbone carbons) rather than the absence of such motions. Indeed, the peak intensity of V213 is recovered as a result of this accelerated fluctuation at the M-like state (see Fig. 8 and Table 1). In any cases, they can be served as hinges to allow possible conformational changes in the transmembrane α-helices B, C, F, and G together with their fluctuation motions (with motional frequency in the order of $<10^4$ Hz), as marked in Table 1. Naturally, higher fluctuation frequency could be expected in the loop region than in the α-helical region, as experimentally noted. Furthermore, it is noteworthy that the V34 intensity of D85N/D96N remains unchanged in spite of the raised pH, in contrast to the case of D85N mutant. This means that the observed intensity-change in the V34 signal of D85N is caused by the dissociation of D96N. In other word, the motional change in the A–B loop in the M-like state could be caused by the dissociation of D96 rather than that of the Schiff base.

Surprisingly, almost all the ^{13}C signals of D85N/V49A are suppressed at pH 10 as illustrated in Fig. 9 but they were recovered again when the pH was lowered [49]. The accelerated conformational fluctuation could be triggered by the presence of open cavity filled with water molecules due to the relaxed helix–helix interactions in the vicinity of V49A in the absence of any van der Waals contact between Lys 216 at the Schiff base and Val 49 residues of the wild type. It was also shown that the peptide C=O of Val 49 forms a hydrogen bond with a water molecule connected to Asp 85 [70]. These observations are obviously the consequence of the fact that the tightly held helices are relaxed by loss of the electrostatic Schiff base–counter ion interaction [18] as a result of protonation to Asp 85 and deprotonation in the Schiff base [71–74].

The present conclusion is consistent with the previous observations, except for the abovementioned motions in the interhelical loops: low-resolution diffraction studies showed the characteristic conformational changes in the M-intermediate occur at helices B and G [15–17,67]. In particular, it was shown that extensive hydrogen-bond network structures are formed for bR near the Schiff base and in the extracellular region, and the center of the active site is a water molecule that receives a hydrogen bond from the positively charged retinal Schiff base and donates hydrogen bonds to Asp 85 and Asp 212, as revealed by the single crystalline X-ray diffraction study [1,13]. The most prominent findings on a single crystalline M state intermediate of D96N mutant [14] are the tilt of the cytoplasmic end of helix F away from the center of the protein and an increase of density of uncertain origin at helix G. In the M state, extensive rearrangement of the 3D network of hydrogen bonded residues and bound water that accounts for the changed pK_a value [67] due to displacements of the side-chains near the retinal induced by its photoisomerization to 13-*cis*, 15-anti. Of course, this might be the essential process to facilitate the proton transfer from the Schiff base by lowering its pK_a value as a result of a breaking hydrogen bonding network. From the refined temperature factors of high-resolution X-ray diffraction, the cytoplasmic ends of helices F and G are disordered between the E–F interhelical loop and residue 176 and beyond residue 222, respectively [13]. Such rearrangement of hydrogen bond network together with disordered structures would be associated with the low-frequency motions we observed at ambient temperature. Consequently, such global low-frequency motions are associated by spontaneous relaxation of the crystalline lattice caused by the abovementioned rearrangement of hydrogen bond network by going from the L to M state.

It is also interesting to note that the ^{13}C NMR spectral pattern of [1-^{13}C]Val-D85N (Fig. 3B) is very similar to that of the deionized blue membrane, including the displaced ^{13}C signals of the transmembrane α-helices, except for the peak positions of V49, V69, and V130, although the individual peaks from the loop region are more broadened in the latter (Fig. 3C). The corresponding ^{13}C NMR peaks [A196 (F–G loop), A160 (E–F loop), A103(C–D loop)] of [3-^{13}C]Ala-labeled D85N were suppressed by interference of the fluctuation frequencies in the order of 10^5 Hz with the proton-decoupling

frequencies [48]. Combined with these data, all the concerned residues in the loop regions became flexible with fluctuation frequency with time scale in the order of 10^4 and 10^5 Hz, due to the absence of bound mono- or divalent cations [62–64] which are essential to hold the transmembrane α-helices together to maintain the secondary structures. More drastic spectral changes, however, especially at the ^{13}C NMR signals of the loop regions, were also observed for [1-^{13}C]Val- or [3-^{13}C]Ala-labeled bacterio-opsin in which retinal was removed [74]. Indeed, Ludlam and Rothchild previously showed a similarity of bR structural changes triggered by chromophore removal and light-driven proton transport, on the basis of FTIR difference spectra [75].

Finally, it is pointed out that ^{13}C NMR signals from the surface areas are almost completely suppressed when [1-^{13}C]Gly-, Ala-, Leu-, Phe-, or Trp-labeled bR preparations were examined because such low-frequency motions are present in these residues coupled with a possible rotation motion of the χ_1 angle around the C_α–C_β bond [35]. Here, the side-chains of these residues can be expressed by the C_α-$C_\beta H_2$-Z. Therefore, interpretation of the spectral data of fully ^{13}C-labeled or site-directed ^{13}C NMR approach utilizing these residues should be made carefully.

6. Concluding remarks and perspective

We demonstrate here that the SRI approach as a function of environmental parameters such as temperature or pH turned out to be a very useful means to locate the portions undergoing low-frequency motions and to evaluate their fluctuation frequencies, as applied for bR and D85N mutants. For this purpose, the identical results are available for such fluctuation frequencies from careful analysis of either [3-^{13}C]Ala- or [1-^{13}C]Val-preparations because the side-chain methyl groups, in the former, undergo free rotation in many cases. In fact, the SRI analysis of site-directed ^{13}C NMR spectra of the 2D crystalline [1-^{13}C]Val- or [3-^{13}C] Ala-labeled bR and D85N mutants, at neutral and alkaline pH, revealed that global low-frequency motions with fluctuation frequencies in the order of 10^4 Hz are induced in the M-like state of D85N mutants. In general, this approach is very important because such motions could be accompanied during the course of the major conformational changes at the active center of protein. Of course, the critical frequency range for the SRI measurement at which the observed ^{13}C signals were recovered or suppressed could be accordingly modified from the points discussed above, if spectra were recorded by either high-frequency MAS or condition of high-power proton-decoupling.

Acknowledgements

We are grateful to Professor J. K. Lanyi of University of California, Irvine, USA and Professor Richard Needleman of Wayne State University, Detroit, USA for providing us mutant strains of bacteriorhodopsin.

References

[1] J.K. Lanyi, Understanding structure and function in the light-driven proton pump bacteriorhodopsin, J. Struct. Biol. 124 (1998) 164–178.
[2] J.K. Lanyi, Bacteriorhodopsin, Annu. Rev. Physiol. 66 (2004) 665–688.
[3] M.S. Braiman, T. Mogi, T. Marti, L.J. Stern, H.G. Khorana, K.J. Rothchild, Vibration spectroscopy of bacteriorhodopsin mutants: light-driven proton transport involves protonation changes of aspartic acid residues 85, 96 and 212, Biochemistry 27 (1988) 8516–8520.
[4] L.S. Brown, J. Sasaki, H. Kandori, A. Maeda, R. Needleman, J.K. Lanyi, Glutamic acid 204 is the terminal proton release group at the extracellular surface of bacteriorhodopsin, J. Biol. Chem. 270 (1995) 27122–27126.
[5] A.K. Dioumaev, H.T. Richter, L.S. Brown, M. Tanio, S. Tuzi, H. Saito, Y. Kimura, R. Needleman, J.K. Lanyi, Existence of a proton transfer chain in bacteriorhodopsin: participation of Glu-194 in the release of protons to the extracellular surface, Biochemistry 37 (1998) 2496–2506.
[6] L.S. Brown, Y. Gat, M. Sheves, Y. Yamazaki, A. Maeda, R. Needleman, J.K. Lanyi, The retinal Schiff base-counterion complex of bacteriorhodopsin: changed geometry during the photocycle is a cause of proton transfer to aspartate 85, Biochemistry 33 (1994) 12001–12011.
[7] N.A. Dencher, D. Dresselhaus, G. Zaccai, G. Büldt, Structural changes in bacteriorhodopsin during proton translocation revealed by neutron diffraction, Proc. Natl. Acad. Sci. U. S. A. 86 (1989) 7876–7879.
[8] T. Hauss, G. Büldt, M.P. Heyn, N.A. Dencher, Light-induced isomerization causes an increase in the chromophore tilt in the M intermediate of bacteriorhodopsin: a neutron diffraction study, Proc. Natl. Acad. Sci. U. S. A. 91 (1994) 11854–11858.
[9] M.H. Koch, N.A. Dencher, D. Oesterhelt, H.J. Plöhn, G. Rapp, G. Büldt, Time-resolved X-ray diffraction study of structural changes associated with the photocycle of bacteriorhodopsin, EMBO J. 10 (1991) 521–526.
[10] M. Nakasako, M. Kataoka, Y. Amemiya, F. Tokunaga, Crystallographic characterization by X-ray diffraction of the M-intermediate from the photo-cycle of bacteriorhodopsin at room temperature, FEBS Lett. 292 (1991) 73–75.
[11] H. Kamikubo, M. Kataoka, G. Váró, T. Oka, F. Tokunaga, R. Needleman, J.K. Lanyi, Structure of the N intermediate of bacteriorhodopsin revealed by X-ray diffraction, Proc. Natl. Acad. Sci. U. S. A. 93 (1996) 1386–1390.
[12] H.J. Sass, I.W. Schachowa, G. Rapp, M.H. Koch, D. Oesterhelt, N.A. Dencher, G. Büldt, The tertiary structural changes in bacteriorhodopsin occur between M states: X-ray diffraction and Fourier transform infrared spectroscopy, EMBO J. 16 (1997) 1484–1491.
[13] H. Luecke, B. Schobert, H.-T. Richter, J.-P. Cartailler, J.K. Lanyi, Structural changes in bacteriorhodopsin during ion transport at 2 angstrom resolution, Science 286 (1999) 255–260.
[14] H. Luecke, B. Schobert, J.-P. Cartailler, H.-T. Richter, A. Rosengarth, R. Needleman, J.K. Lanyi, Coupling photoisomerization of retinal to directional transport in bacteriorhodopsin, J. Mol. Biol. 300 (2000) 1237–1255.
[15] S. Subramaniam, M. Gerstein, D. Oesterhelt, R. Henderson, Electron diffraction analysis of structural changes in the photocycle of bacteriorhodopsin, EMBO J. 12 (1993) 1–8.
[16] S. Subramaniam, M. Lindahl, P. Bullough, A.R. Faruqi, J. Tittor, D. Oesterhelt, L. Brown, J.K. Lanyi, R. Henderson, Protein conformational changes in the bacteriorhodopsin photocycle, J. Mol. Biol. 287 (1999) 145–146.
[17] J. Vonck, A three-dimensional difference map of the N intermediate in the bacteriorhodopsin photocycle: part of the F helix tilts in the M to N transition, Biochemistry 35 (1996) 5870–5878.
[18] M. Kataoka, H. Kamikubo, F. Tokunaga, L.S Brown, Y. Yamazaki, A. Maeda, M. Sheves, R. Needleman, J.K. Lanyi, Energy coupling in an ion pump. The reprotonation switch of bacteriorhodopsin, J. Mol. Biol. 243 (1994) 621–638.
[19] J.K. Lanyi, Mechanism of ion transport across membranes. Bacteriorhodopsin as a prototype for proton pumps, J. Biol. Chem. 272 (1997) 31209–31212.
[20] A.E. Blaurock, W. Stoeckenius, Structure of the purple membrane, Nature New Biol. 233 (1971) 152–155.
[21] J.M. Baldwin, R. Henderson, E. Beckman, F. Zemlin, Images of purple membrane at 2.8 A resolution obtained by cryo-electron microscopy, J. Mol. Biol. 202 (1988) 585–591.
[22] H. Saitô, S. Tuzi, S. Yamaguchi, M. Tanio, A. Naito, Conformation and backbone dynamics of bacteriorhodopsin revealed by ^{13}C-NMR, Biochim. Biophys. Acta 1460 (2000) 39–48.
[23] S. Yamaguchi, S. Tuzi, K. Yonebayashi, A. Naito, R. Needleman, J.K. Lanyi, H. Saitô, Surface dynamics of bacteriorhodopsin as revealed by ^{13}C NMR studies on [^{13}C] Ala-labeled proteins: detection of millisecond or microsecond motions in interhelical loops and C-terminal α-helix, J. Biochem. 129 (2001) 373–382.
[24] S. Yamaguchi, K. Yonebayashi, H. Konishi, S. Tuzi, A. Naito, J.K. Lanyi, R. Needleman, H. Saitô, Cytoplasmic surface structure of bacteriorhodopsin consisting of interhelical loops and C-terminal alpha helix, modified by a variety of environmental factors as studied by ^{13}C-NMR, Eur. J. Biochem. 268 (2001) 2218–2228.
[25] K. Yonebayashi, S. Yamaguchi, S. Tuzi, H. Saitô, Cytoplasmic surface structures of bacteriorhodopsin modified by site-directed mutations and cation binding as revealed by ^{13}C NMR, Eur. Biophys. J. 32 (2003) 1–11.
[26] H. Saitô, S. Yamaguchi, K. Ogawa, S. Tuzi, M. Marquez, C. Sanz, E. Padros, Glutamic acid residues of bacteriorhodopsin at the extracellular surface as determinants for conformation and dynamics as revealed by site-directed solid-state ^{13}C NMR, Biophys. J. 86 (2004) 1673–1681.
[27] H. Saitô, I. Ando, A. Naito, Solid State NMR Spectroscopy for Biopolymers: Principles and Applications, Springer, 2006.
[28] H. Saitô, Site directed solid state NMR on membrane proteins, Annu. Rep. NMR Spectrosc. 57 (2006) 99–175.
[29] N. Grigorieff, T.A. Ceska, K.H. Dowing, J.M. Baldwin, R. Henderson, Electron-crystallographic refinement of the structure of bacteriorhodopsin, J. Mol. Biol. 259 (1996) 393–421.
[30] E. Pebay-Peyroula, G. Rummel, J.P. Rosenbusch, E.M. Landau, X-ray structure of bacteriorhodopsin at 2.5 angstroms from microcrystals grown in lipidic cubic phases, Science 277 (1997) 1676–1681.
[31] H. Luecke, H.T. Richter, J.K. Lanyi, Proton transfer pathways in bacteriorhodopsin at 2.3 angstrom resolution, Science 280 (1998) 1934–1937.
[32] L. Essen, R. Siegert, W.D. Lehmann, D. Oesterhelt, Lipid patches in membrane protein oligomers: crystal structure of the bacteriorhodopsin-lipid complex, Proc. Natl. Acad. Sci. U. S. A. 95 (1998) 11673–11678.
[33] H. Sato, K. Takeda, K. Tani, T. Hino, T. Okada, M. Nakasako, N. Kamiya, T. Kouyama, Specific lipid-protein interactions in a novel honeycomb lattice structure of bacteriorhodopsin, Acta Crystallogr., D 55 (1999) 1251–1256.
[34] S. Tuzi, S. Yamaguchi, A. Naito, R. Needleman, J.K. Lanyi, H. Saitô, Conformation and dynamics of [3-^{13}C]Ala-labeled bacteriorhodopsin and bacterioopsin, induced by interaction with retinal and its analogs, as studied by ^{13}C nuclear magnetic resonance, Biochemistry 35 (1996) 7520–7527.
[35] H. Saitô, J. Mikami, S. Yamaguchi, M. Tanio, A. Kira, T. Arakawa, K. Yamamoto, S. Tuzi, Site-directed ^{13}C solid-state NMR studies on membrane proteins: strategy

and goals toward revealing conformation and dynamics as illustrated for bacteriorhodopsin labeled with [1-^{13}C]amino acid residues, Magn. Reson. Chem. 42 (2004) 218–230.
[36] H. Saitô, T. Tsuchida, K. Ogawa, T. Arakawa, S. Yamaguchi, S. Tuzi, Residue-specific millisecond to microsecond fluctuations in bacteriorhodopsin induced by disrupted or disorganized two-dimensional crystalline lattice, through modified lipid–helix and helix–helix interactions, as revealed by ^{13}C NMR, Biochim. Biopys. Acta 1565 (2002) 97–106.
[37] H. Saitô, K. Yamamoto, S. Tuzi, S. Yamaguchi, Backbone dynamics of membrane proteins in lipid bilayers: the effect of two-dimensional array formation as revealed by site-directed solid-state ^{13}C NMR studies on [3-^{13}C]Ala- and [1-^{13}C] Val-labeled bacteriorhodopsin, Biochim. Biopys. Acta 1616 (2003) 127–136.
[38] H. Saitô, Dynamic pictures of membrane proteins in two-dimensional crystal, lipid bilayer and detergent as revealed by site-directed solid-state ^{13}C NMR, Chem. Phys. Lipids 132 (2004) 101–112.
[39] H. Saitô, Y. Kawase, A. Kira, K. Yamamoto, M. Tanio, S. Yamauchi, S. Tuzi, A. Naito, Surface and dynamic structures of bacteriorhodopsin in a 2D crystal, a distorted or disrupted lattice, as revealed by site-directed solid-state ^{13}C NMR, Photochem. Photobiol. 83 (2007) 253–262.
[40] D. Suwelack, W.P. Rothwell, J.S. Waugh, Slow molecular motion detected in the NMR spectra of rotating solids, J. Chem. Phys. 73 (1980) 2559–2569.
[41] W.P. Rothwell, J.S. Waugh, Transverse relaxation of dipolar coupled spin systems under rf irradiation: detecting motions in solids, J. Chem. Phys. 74 (1981) 2721–2732.
[42] A.G. Palmer III, C.D. Kroenke, J.P. Loria, Nuclear magnetic resonance methods for quantifying microsecond-to-millisecond motions in biological macromolecules, Meth. Enzymol. 339 (2001) 204–238.
[43] M. Akke, NMR methods for characterizing microsecond to millisecond dynamics in recognition and catalysis, Curr. Opin. Struct. Biol. 12 (2002) 642–647.
[44] A.G. Palmer III, Probing molecular motion by NMR, Curr. Opin. Struct. Biol. 7 (1997) 732–737.
[45] H. Saitô, Conformation-dependent ^{13}C chemical shifts: a new means of conformational characterization as obtained by high-resolution solid-state NMR, Magn. Reson. Chem. 24 (1986) 835–852.
[46] H. Saitô, I. Ando, High-resolution solid-state NMR studies of synthetic and biological macromolecules, Annu. Rep. NMR Spectrosc. 21 (1989) 209–290.
[47] D.-K. Lee, A. Ramamoorthy, Determination of the solid conformation of polyalanine using magic-angle spinning NMR spectroscopy, J. Phys. Chem. B103 (1999) 271–275.
[48] Y. Kawase, M. Tanio, A. Kira, S. Yamaguchi, S. Tuzi, A. Naito, M. Kataoka, J.K. Lanyi, R. Needleman, H. Saitô, Alteration of conformation and dynamics of bacteriorhodopsin induced by protonation of Asp 85 and deprotonation of Schiff base as studied by ^{13}C NMR, Biochemistry 39 (2000) 14472–14480.
[49] A. Kira, M. Tanio, S. Tuzi, H. Saitô, Significance of low-frequency local fluctuation motions in the transmembrane B and C α-helices of bacteriorhodopsin, to facilitate efficient proton uptake from the cytoplasmic surface, as revealed by site-directed solid-state ^{13}C NMR, Eur. Biophys. J. 33 (2004) 580–588.
[50] I. Kawamura, M. Ohmine, J. Tanabe, S. Tuzi, H. Saitô, A. Naito, Dynamic aspects of extracellular loop region as a proton release pathway of bacteriorhodopsin studied by relaxation time measurements by solid state NMR, Biochim. Biophys. Acta 1768 (2007) 3090–3097.
[51] H. Onishi, M.E. McCance, N.E. Gibbons, A synthetic medium for extremely halophilic bacteria, Can. J. Microbiol. 11 (1965) 365–373.
[52] D. Oesterhelt, W. Stoeckenius, Isolation of the cell membrane of *Halobacterium halobium* and its fractionation into red and purple membrane, Methods Enzymol. 31 (1974) 667–678.
[53] S. Tuzi, S. Yamaguchi, M. Tanio, H. Konishi, S. Inoue, A. Naito, R. Needleman, J.K. Lanyi, H. Saitô, Location of a cation-binding site in the loop between helices F and G of bacteriorhodopsin as studied by ^{13}C NMR, Biophys. J. 76 (1999) 1523–1531.
[54] A. Naito, A. Fukutani, M. Uitdehaag, S. Tuzi, H. Saitô, Backbone dynamics of polycrystalline peptides studied by measurements of ^{15}N NMR lineshapes and ^{13}C transverse relaxation times, J. Mol. Struc. 441 (1998) 231–241.
[55] E.O. Stejskal, H.S. Gutowsky, Proton magnetic resonance of the CH_3 Group. IV. Calculation of the tunneling frequency and of T_1 in solids, J. Chem. Phys. 28 (1958) 388–394.
[56] D.W. Woessner, Spin relaxation processes in a two-proton system undergoing anisotropic reorientation, J. Chem. Phys. 36 (1962) 1–4.
[57] Ch. Brevard, J.P. Kintzinger, J.M. Lehn, Molecular dynamics: VII. Component analysis of local molecular motions, Tetrahedron 28 (1972) 2447–2460.
[58] A. Naito, S. Ganapathy, K. Akasaka, C.A. McDowell, Spin-lattice relaxation of ^{13}C in solid amino acids using the CP-MAS technique, J. Magn. Reson. 54 (1983) 226–235.
[59] P. Barré, S. Yamaguchi, H. Saitô, Backbone dynamics of bacteriorhodopsin as studied by ^{13}C solid-state NMR spectroscopy, Eur. Biophys. J. 32 (2003) 578–584.
[60] D.K. Lee, J.S. Santos, A. Ramamorthy, Application of one-dimensional dipolar shift solid state NMR spectroscopy to study the backbone conformation of membrane-associated peptides in phospholipids bilayers, J. Phys. Chem. B103 (1999) 8383–8390.
[61] S. Tuzi, A. Naito, H. Saitô, Temperature-dependent conformational change of bacteriorhodopsin as studied by solid-state ^{13}C NMR, Eur. J. Biochem. 239 (1996) 294–301.
[62] S. Tuzi, J. Hasegawa, R. Kawaminami, A. Naito, H. Saitô, Regio-selective detection of dynamic structure of transmembrane α-helices as revealed from ^{13}C NMR spectra of [3-^{13}C]Ala-labeled bacteriorhodopsin in the presence of Mn^{2+} ion, Biophys. J. 81 (2001) 425–434.
[63] T.A. Moore, M.E. Edgerton, G. Parr, C. Greenwood, R.N. Perham, Studies of an acid-induced species of purple membrane from *Halobacterium halobium*, Biochem. J. 171 (1978) 469–476.
[64] P.C. Mowery, R.H. Lozier, Q. Chae, Y.W. Tseng, M. Taylor, W. Stoeckenius, Effect of acid pH on the absorption spectra and photoreactions of bacteriorhodopsin, Biochemistry 18 (1979) 4100–4107.
[65] C.H. Chang, J.G. Chen, R. Govindjee, T. Ebrey, Cation binding by bacteriorhodopsin, Proc. Natl. Acad. Sci. U. S. A. 82 (1985) 396–400.
[66] S. Tuzi, A. Naito, H. Saitô, Local protein structure and dynamics at kinked transmembrane α-helices of [1-^{13}C]Pro-labeled bacteriorhodopsin as revealed by site-directed solid-state ^{13}C NMR, J. Mol. Struct. 654 (2003) 205–214.
[67] H. Luecke, B. Schobert, H.T. Richter, J.P Cartailler, J.K. Lanyi, Structure of bacteriorhodopsin at 1.55 A resolution, J. Mol. Biol. 291 (1999) 899–911.
[68] D.A. Torchia, J.R. Lyerla, Molecular mobility of polypeptides containing proline as determined by ^{13}C magnetic resonance, Biopolymers 13 (1974) 97–114.
[69] I. Ando, H. Saitô, R. Tabeta, A. Shoji, T. Ozaki, Conformation-dependent chemical shifts of poly(L-alanine) in the solid state: PFT INDO calculation of *N*-acetyl-*N*′-methyl-L-alanine amide as a model compound of poly(L-alanine), Macromolecules 17 (1984) 457–461.
[70] Y. Yamazaki, S. Tuzi, H. Saitô, H. Kandori, R. Needleman, J.K. Lanyi, A. Maeda, Hydrogen bonds of water and C=O groups coordinate long-range structural changes in the L photointermediate of bacteriorhodopsin, Biochemistry 35 (1996) 4063–4068.
[71] J.K. Lanyi, B. Schobert, Crystallographic structure of the retinal and the protein after deprotonation of the Schiff Base: the switch in the bacteriorhodopsin photocycle, J. Mol. Biol. 321 (2002) 727–737.
[72] H. Kamikubo, T. Oka, Y. Imamoto, F. Tokunaga, J.K. Lanyi, M. Kataoka, The last phase of the reprotonation switch in bacteriorhodopsin: the transition between the M-type and the N-type protein conformation depends on hydration, Biochemistry 36 (1997) 12282–12287.
[73] L. Brown, A.K. Dioumaev, R. Niedleman, J.K. Lanyi, Local-access model for proton transfer in bacteriorhodopsin, Biochemistry 37 (1998) 3982–3993.
[74] S. Yamaguchi, S. Tuzi, M. Tanio, A. Naito, J.K. Lanyi, R. Needleman, H. Saitô, Irreversible conformational change of bacterio-opsin induced by binding of retinal during its reconstitution to bacteriorhodopsin, as studied by ^{13}C NMR, J. Biochem. 27 (2000) 861–869.
[75] G.J Ludlam, K.J. Rothschild, Similarity of bacteriorhodopsin structural changes triggered by chromophore removal and light-driven proton transport, FEBS Lett. 407 (1997) 285–288.